The Mw 6.3, 2009 L'Aquila earthquake: source, path and site effects from spectral analysis of strong motion data

D. Bindi, F.Pacor, L. Luzi, M.Massa and G. Ameri.
Istituto Nazionale di Geofisica e Vulcanologia, Milan, bindi@mi.ingv.it

Strong-motion data set

For this work, we analyzed 264 recordings from 56 strong-motion stations triggered by the 2009 April 6, L'Aquila earthquake and 12 aftershocks (Tab.1). These stations belong to the Italian Strong Motion Network (RAN), managed by the Italian Department of Civil Protection (DPC).

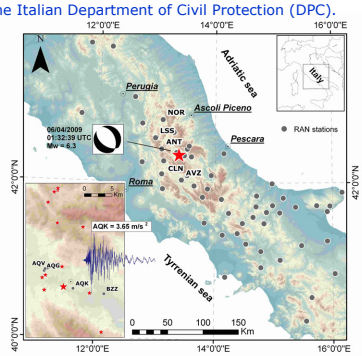

Fig.1 - Map showing the epicentres of considered earthquakes (red stars) and recording stations (grey circles); the main shock recording at station AQK is also displayed. The focal solution is taken from the Global Centroid Moment Tensor Project (http://www.globalcmt.org)

ABSTRACT

The strong motion data of April 6, 2009 L'Aquila (Central Italy) earthquake (M_w=6.3) and of 12 aftershocks (4.1≤M_w≤5.6) recorded by 56 stations of the Italian strong motion network are spectrally analyzed to estimate the source parameters, the seismic attenuation, and the site amplification effects. The obtained source spectra for S-wave have stress drop values ranging from 2.4 to 16.8 MPa, being the stress drop of the main shock equal to 9.2MPa. The spectral curves describing the attenuation with distance show the presence of shoulders and bumps, mainly around 50 and 150km, as consequence of significant reflected and refracted arrivals from crustal interfaces. The attenuation in the first 50 km is well described by a quality factor equal to $Q(f)=59f^{0.56}$ obtained by fixing the geometrical spreading exponent to 1. Finally, the horizontal-to-vertical spectral ratio provides unreliable estimates of local site effects for those stations showing large amplifications over the vertical component of motion.

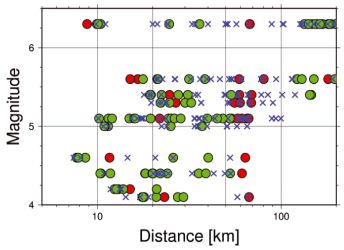

Fig. 2 – Moment magnitude versus hypocentral distance distribution of the considered recordings. The site classification accordingly to the Eurocode8 is shown with different symbols (crosses: class A; green filled circles: class B; red filled circles: class C).

Tab.1 – Source parameters of the considered earthquakes. $M_w^{(est)}$ is the moment magnitude computed starting from the seismic moment Mo estimated in this work.

Id	Event Date yymmdd_hhmmss	^+M_w	$M_w^{(est)}$	Mo [Nm]	f_c [Hz]	Ro [km]	Δσ [MPa]	$\Delta\sigma_{RMS}$ [MPa]
1	20090406_013239	6.3	6.3	3.42e+18*	0.24	5.46	9.2	10.7
2	20090406_023704	5.1	4.8	2.10 e+16	1.39	0.94	11.3	13.4
3	20090406_163809	4.4	4.3	3.17e+15	2.15	0.61	6.2	7.8
4	20090406_231537	5.1	4.8	1.90 e+16	1.56	0.84	14.3	16.5
5	20090407_092628	5.0	4.8	1.74 e+16	1.32	0.99	7.8	9.3
6	20090407_174737	5.6	5.5	2.52e+17*	0.70	1.87	16.8	20.0
7	20090407_213429	4.6	4.5	8.25e+15	1.39	0.93	4.4	4.6
8	20090408_225650	4.1	4.1	1.85e+15	2.97	0.44	9.6	9.6
9	20090409_005259	5.4	5.4	1.60e+17*	0.70	1.86	10.9	15.6
10	20090409_031452	4.4	4.4	5.55e+15	2.14	0.61	10.7	10.6
11	20090409_043244	4.2	4.4	4.70e+15	1.38	0.94	2.4	2.5
12	20090409_193816	5.3	5.2	7.50e+16*	0.87	1.49	9.8	17.3
13	20090413_211424	5.1	4.8	1.84e+16	1.36	0.96	9.2	10.3

Method

We apply a two-step non-parametric approach (GIT) (e.g. Castro *et al.* 1990; Oth *et al.* 2008) to describe the observed spectral amplitudes $D(f,r)$ in terms of source $S(f)$, attenuation $A(f,r)$ and site $Z(f)$ contributions.

$$\log_{10} D(f,r_{ij}) = \log_{10} A(f,r_{ij}) + \log_{10} \tilde{S}_j(f) \quad (1)$$

$$\log_{10} R(f,r_{ij}) = \log_{10} Z_i + \log_{10} S_j(f) \quad (2)$$

where r is the hypocentral distance, f the frequency, i=1…Nsta spans the set of available stations, j=1…Neve spans the set of considered earthquakes, $\tilde{S}_j(f)$ is a scalar which depends on the size of the j-th source and $R(f,r_{ij})$ represents the observed spectral values corrected for attenuation $A(f,r_{ij})$. Considering the whole set of available recordings, equations (1) and (2) define two linear systems that we solved in a least-squares sense. In the first step, the attenuation-with-distance curves $A(f,r)$ are obtained by solving the linear system (1). The inversion is performed for each frequency and the distance range is discretized into M bins Δr km wide. In the second step, the residuals $R(f,r_{ij})$ are used to determine the source spectra $S_j(f)$ and the site amplification functions $Z_i(f)$ by solving system (2), without assuming any a-priori functional form to describe the source spectra. A standard source model (Brune, 1970) is later fit to the non-parametric solutions to determine the source parameters.

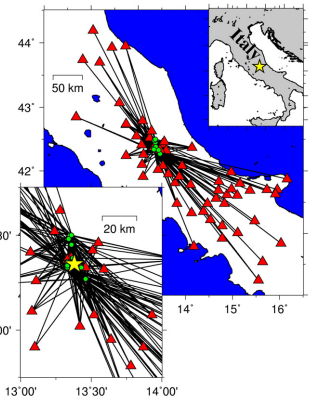

Fig. 3 – Path coverage for the stations (triangles) and earthquakes (circles) analyzed in the manuscript. The star indicates the epicentre of the main shock.

Spectral Attenuation with distance

The first step of the inversion allows us to determine the spectral attenuation curves $A(f,r)$ as function of distance.

Fig. 4 (**top panel**) shows the $A(f,r)$ curves. The rate of attenuation with distance varies over the analyzed distance range. In particular, the curves decay in the first 50 km, then they flat or slope upward depending on the frequency value. For distances larger than about 70 km the curves generally decay with distance less rapidly than in the first 50 km. Finally, for distances from 100 to 150 km and frequency smaller than 2 Hz, the spectral attenuation curves have small bumps. The behavior of the spectral attenuation curves suggests that reflections and refractions from crustal interfaces are significant in the investigated area for distances between 50 and 70 km and around 150 km.

The quality factor Q for S waves is estimated selecting only recordings at distances in the range 5–50 km, where a monotonic attenuation with distance occurs.
The attenuation curves are described in terms of geometrical and anelastic attenuation, considering the following model and constraining the geometrical spreading coefficient n=1 :

$$A(f,r) = \left(\frac{8.5}{r}\right)^n \exp\left[\frac{-\pi f (r-8.5)}{\beta Q}\right]$$

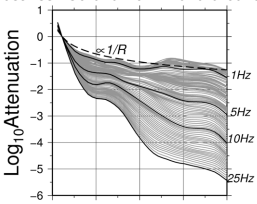

Fig.4 – Top. Non-parametric S-wave spectral attenuation versus distance (grey curves). The results for four selected frequencies are shown as black lines. The decay proportional to the inverse of distance (dashed line) is shown for reference.
Bottom. Frequency dependence of the quality factor Q for distances between 6 and 50 km (grey line) and best least-square fitting model (black line). The value of the geometrical spreading exponent is fixed to n = 1.

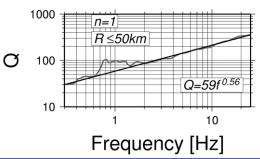

Site effects

In the second step, the observed spectral amplitudes, corrected for attenuation, are inverted to separate the source contribution from the site amplification effects. System (2) is solved constraining to zero the logarithm sum of the site amplification functions Z(f) of two rock sites, namely Celano (CLN) and Leonessa (LSS)

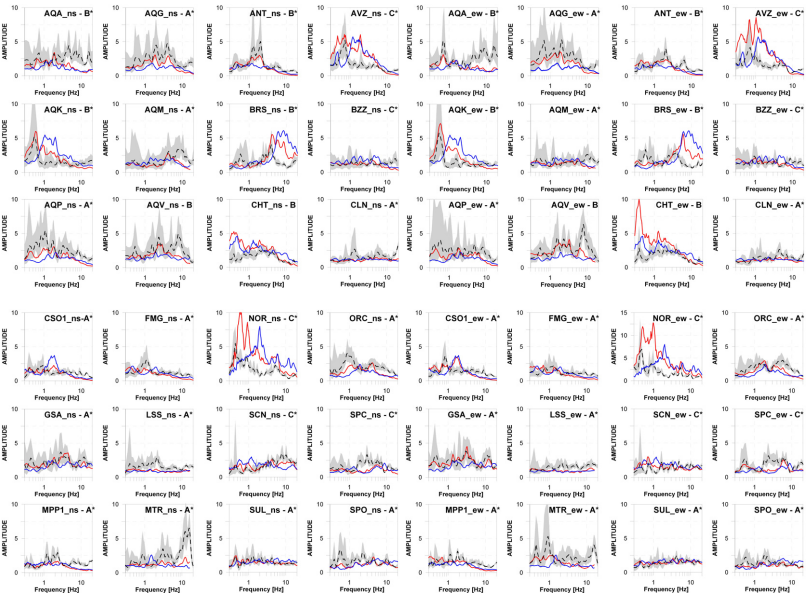

Fig.6 - Site amplification effects estimated for 24 different stations. The station name and the relevant site classification, selected accordingly to the EC8, is given in the upper right corner of each panel. The average (black dashed line) ±1SD (grey area) of the NS or EW to vertical spectral ratios are compared with the GIT results for the NS or EW (red) and vertical (blue) components

Source Functions

The non-parametric source functions obtained for each component are composed into a single source spectrum for each earthquake to determine the S-wave source parameters. Then, the source parameters are computed by fitting, in a least-squares sense, a standard ω-square model.

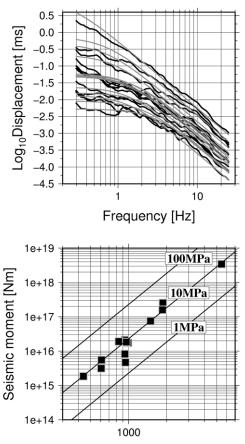

Fig.7 - Top panel: displacement source spectra (black lines) obtained from inversion and best fit Brune models (grey lines).
Bottom panel: Seismic moment versus source radius (squares), compared with constant-stress drop predictions (black lines).

The estimated corner frequency for the main shock is 0.24 Hz, corresponding to a Brune radius of 5.46 km and a stress drop of 9.2 MPa. The stress drop of the 13 considered earthquakes varies between 2.4 and 16.8 MPa.

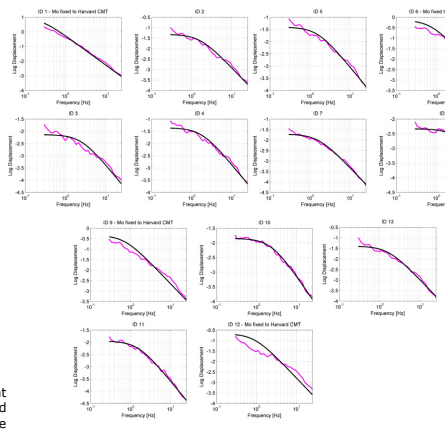

Fig.8 - Source spectra obtained by applying the GIT inversion (purple) and best fit Brune model (black). Each panel shows the fit for a different earthquake, being the ID the same as in Table 1. The earthquakes for which the seismic moment has been constrained to the valued provided by Harvard-CMT are also indicated.

References

- Brune, J.N., 1970. Tectonic stress and the spectra of seismic shear waves from earthquakes. J. Geophys. Res. 75, 4997–5009.
-Castro, R. R., Anderson, J. G.&. Singh, S.K., 1990. Site response attenuation and source spectra of S waves along the Guerrero, Mexico, subduction zone, Bull. Seism. Soc. Am. 80, 1481–1503.
- Oth, A., D. Bindi, S. Parolai, and F. Wenzel (2008). S-wave attenuation characteristics beneath the Vrancea region in Romania: new insights from the inversion of ground-motion spectra, Bull. Seismol. Soc. Am. 98, no. 5, 2482–2497, doi: 10.1785/0120080106.